Published in final edited form as:
Optom Vis Sci. 2012 November ; 89(11): 1590–1600. doi:10.1097/OPX.0b013e31826cfae5.

Scale and Spatial Distribution of Optical Aberrations Associated with Tear Break-up

Nikole L. Himebaugh, OD, PhD, **Jayoung Nam, PhD**, **Arthur Bradley, PhD**, **Haixia Liu, PhD**, **Larry N. Thibos, PhD, FAAO**, and **Carolyn G. Begley, OD, MS, FAAO**
Indiana University School of Optometry, 800 E. Atwater Avenue, Bloomington, IN 47405

Abstract

Purpose—We examined the spatial correlation between tear break up (TBU) and the associated optical anomalies on multiple spatial scales.

Methods—Five subjects refrained from blinking while the time course and patterns of TBU were sequentially observed using fluorescein (FL), retroillumination (RI), and Shack-Hartmann (SH) aberrometry. Wavefront error maps were developed using Zernike polynomials, as well as local zonal analysis of measured wavefront slopes. The difference between these maps reveals the presence of very high order aberrations missed by standard modal fitting methods. Size of SH spots was also quantified to estimate optical perturbations on a microscopic scale. The spatial correlation between TBUand optical aberrations was also computed.

Results—Degradation of the tear film increased wavefront aberrations over all spatial scales measured. Consistent with tear thinning, blink suppression induced an irregular pattern of phase advances in regions of TBU. SH spot size also increased in regions of TBU, which indicates the presence of optical aberrations on a scale smaller than individual lenslets.

Conclusions—The optical signature of TBU caused by blink suppression is a combination of wavefront aberrations on macroscopic and microscopic scales due to nonuniform tear film thinning and possible exposure of a rough epithelial surface. Localized optical 2 defects correspond temporally and spatially with TBU revealed by FL and RI. In addition to gross wavefront aberrations, scatter develops in areas of TBU that will further contribute to image degradation and visual disturbances following TBU.

Keywords

tear film stability; tear film break-up; optical aberrations; Shack-Hartmann aberrometry; scatter

The ocular surface provides the main focusing power for the eye, but its optical quality relies primarily on the integrity of the tear film which forms the first and most powerful refracting surface of the eye.[1] When the tear film disrupts locally, a phenomenon known as tear film break-up (TBU), non-uniformities in tear film thickness are created,[2] resulting in an irregular optical surface and characteristic increases in higher order aberrations (HOA)with an accompanying reduction in image quality.[3-9] Tear instability can also precipitate significant reductions in visual acuity and contrast sensitivity.[4,10-14] The optical disturbances associated with TBU are thought to generate the visual disturbances common among dry eye patients, contact lens wearers and post-refractive surgery patients.[14-18]

Corresponding author: Nikole L. Himebaugh, Indiana University School of Optometry, 800 E. Atwater Ave., Bloomington, IN 47405, Office: (812) 856-5977, Fax: (812) 855-7045 nhimebau@indiana.edu.

Commercial relationship disclosure: None. No conflicts of interest.

Recently, visual disturbance has been added to the definition of dry eye[19] in recognition of the optical effect of tear instability and its impact on vision and quality of life among dry eye patients.[20-22]

The increase in HOA associated with TBU are typically quantified by a Zernike polynomial fit up to the 6th or 10th order.[6,8,9] However, there is evidence that increased HOAs characterized by these Zernike polynomials are not the only optical changes caused by TBU.[4] One measure of the magnitude of those aberrations not included in a Zernike description is the RMS fit error between wavefront slope measurements and fitted Zernike polynomials.[4,23] These additional aberrations, called very high order aberrations (VHOA), represent optical disturbances on a spatial scale measurable by current Shack-Hartmann (SH) technology but finer than 6th to 10th order Zernike polynomials.[4,24] In addition, TBU causes optical disturbances that are too fine to be resolved by a clinical SH aberrometer.[24] These very fine scale “micro-aberrations” scatter light,[25] thereby blurring the spot images formed by individual lenslets in a SH wavefront sensor.[24] For the same reason, scattered light causes the double pass point-spread function (PSF) for the whole eye to contain a disproportionate amount of light outside of the central core.[26] Thus, light scatter associated with micro-aberrations further reduces retinal image quality[24] and potentially hampers vision during late stages of TBU.

To evaluate these numerous effects of TBU that exist over multiple spatial scales optical changes were measured over relatively long periods of blink suppression in order to reveal the full range of optical disturbances associated with TBU. The resulting analysis allowed a determination of the spatial correlation between optical disturbances and areas of TBU. Although the temporal evolution of aggregate changes in optical aberrations with tear film instability have been studied previously,[4,8,27] this study emphasizes the spatial correlation between individual areas of TBU and the resulting local changes in aberrations over multiple spatial scales.

METHODS

Rationale

The SH wavefront aberrometer measures wavefront aberrations at a multitude of locations in the eye’s pupil simultaneously.[28] This is achieved by using an array of small lenslets to focus a corresponding array of images from reflected light produced by a quasi-point source on the fundus. A schematic representation of this array of spot images is shown in Figure 1. Images captured experimentally are the raw data from which optical disturbances produced by TBU were quantified. Conventional analysis of the SH data image measures spot displacement from the optical axis of the corresponding lenslet to calculate mean wavefront slope over the face of each lenslet. Slope measurements may be converted to wavefront phase error two ways. Modal reconstruction uses the method of least squares to fit slope data with a weighted sum of the spatial derivatives of Zernike polynomials. In theory, a modal reconstruction may include as many polynomial modes as there are spots, which is equal to the number of lenslets covering the eye’s pupil. However, clinical aberrometers typically use only a subset of modes from the 1st order to the 6th (or at most 10th) order when quantifying ocular aberrations. Orders 1-2 are called lower-order aberrations (LOA) and orders 3-6 (or 3-10) are called HOAs. A wavefront error map made from LOA plus HOA is a smooth surface that may fail to include the highly irregular, localized defects characteristic of TBU.[29] To capture these missing features a second wavefront analysis method was used, known as zonal reconstruction, that integrates individual slope measurements to calculate the map of wavefront phase errors (WFE).[30] Zonal reconstruction avoids smoothing and therefore it captures local aberrations on a spatial scale finer than modal fitting methods. However, a disadvantage of zonal reconstruction is that the wavefront map is defined only at

the sample points corresponding to the lenslet centers. Interpolating these sample points onto a finer grid covering the face of individual lenslets requires additional assumptions for the zonal method, whereas evaluating the Zernike polynomials on a finer grid provides interpolation of the modal wavefront without further assumptions.

Spatial scales of optical aberrations resolvable by the aberrometer are tightly linked to the lenslet size used in a SH aberrometer (Figure 1). Lenslets are used to sample the pupil over tightly-packed discrete areas with center-to-center spacing equal to lenslet diameter. Mean wavefront slopes measured over this sampling array are fitted with a finite series of Zernike functions by least squares fitting method (LSQ). Consequently, the maximum number of Zernike functions (or "modes") is limited by the number of samples, which in turn is limited by lenslet size (Figure 1). For example, when the lenslet diameter is 0.4 mm, around 178 sample points are available for a circular pupil of radius 3 mm. For this configuration, modes beyond the 18^{th} order (2^{nd} through 18^{th} orders will contain 187 modes) cannot be included in the reconstruction. Even fewer modes are captured in practice because the quality of the LSQ fit improves for an over-determined system where the number of data points is larger than the number of modes.[31] Therefore, the higher-order modes reported by clinical aberrometers typically include fewer modes than are theoretically possible.

In this report, the term "very high order aberrations (VHOA)" has been used to represent Zernike orders extending from the highest HOA fit to the data to an upper limit set by lenslet diameter.[24] RMS fitting error[4,23] is a scalar measure of the combined magnitude of all VHOA over the entire pupil. Since zonal reconstructions include HOA and VHOA, but modal reconstructions include only HOA, the algebraic difference between these two wavefront error maps represents VHOA. As depicted in Figure1, the term "macro-aberrations" has been used to designate the complete range of resolvable modes from LOA to VHOA. Beyond the resolution limit set by lenslet diameter lies the domain of "micro" aberrations that produce significant variation of wavefront phase over the face of individual lenslets without changing mean slope. These micro-aberrations are typically present within areas of TBU and they cause spot enlargement (rather than spot displacement) because they scatter light.[24,25] One of the primary goals of this current study was to determine the extent to which TBU generates optical disturbances in the two finer scales of aberrations not included in conventional modal analysis of HOA, namely the macro-VHOA and micro-aberrations.

Subjects

Thestudy design followed the tenets of the Declaration of Helsinki and was approved by the Institutional Review Board at Indiana University. Informed consent was obtained from all subjects. Measurements were obtained from five normal subjects (3 females and 2 males) between the ages of 24-45. Individual subjects are identified in this report using the subject number given in Table 1. None of the subjects had been diagnosed with dry eye or any other ocular condition, none reported anything other than very infrequent dry eye symptoms, and all had a tear break-up time of > 10 seconds and a Schirmer's tear test of >5mm in 5 minutes.

Apparatus and Experimental Design

Two methods were used in this study to monitor TBU, the traditional sodium fluorescein method (FL)[32] and a non-invasive technique involving retroillumination of the tear film (RI).[29] Optical aberrations of the whole eye were measured using a SH aberrometer. These three methods were used to sequentially measure TBU and monochromatic aberrations during periods of extended blink suppression. The traditional FL method for observing TBU was performed with wide beam (30 deg.) illumination of the eye with a cobalt-blue light

source. The tear film was viewed and recorded with a Zeiss biomicroscope system (8× magnification) fitted with a Wratten #8 filter. FL was instilled using a FL sodium ophthalmic strip (Akorn, Inc., Buffalo Grove, IL) moistened with non-preserved saline. To obtain the RI image of the full pupil, the light source on the Zeiss biomicroscope was positioned immediately adjacent to the aperture of the channel containing a video camera, as described previously.[4,10,29]

A SH aberrometer, described elsewhere in detail,[1,33,34] was used to measure optical aberrations of the whole eye before and after TBU. The light source was 633 nm and contained a micro-lenslet array (0.4mm center-to-center spacing, 24mm focal length), positioned conjugate to the plane of the eye's entrance pupil by a unit magnification relay telescope. This configuration provided approximately 180 measurements of wavefront slope over a 6 mm pupil.

Procedures

The right eye of each subject was dilated with 0.5% tropicamide to maximize the area of the cornea and overlying tear film that could be visualized and studied by the RI and SH methods. Both eyes were anesthetized with 0.5% proparacaine to minimize discomfort during blink suppression and to prevent reflexive tearing and blinking. Because the purpose of this study was to extend TBU to obtain a full range of optical aberrations,the tear film was monitored well beyond the first break.

The aberrometer was immediately adjacent to the biomicroscope (used to monitor both RI and FL images), and subjects altered head position from one instrument to the next. For FL and RI measurements, the subject's head was positioned and stabilized using a standard biomicroscope headrest. Baseline SH measurements were obtained just after a blink. For each subject, the experiment began by monitoring TBU with the RI technique. When intensity fluctuations in the RI image were clearly evident, the light source on the biomicroscope was switched to cobalt blue to record tear film fluorescence. The subject then rotated his or her head without blinking to view through the adjacent SH aberrometer for a single measurement. A short training session was sufficient to master this protocol.

Optical Analysis

The spot displacements in the SH aberrometer were converted into WFE maps using custom-designed MATLAB® (The MATHWORKS™, Natick, MA) programs.[1,28] that use the raw wavefront slopes measured by the aberrometer to develop both modal and zonal wavefronts. A pupil size of 6 mm was used for WFE analysis. Modal maps were interpolated with Zernike polynomials to produce [101×101] arrays of phase values over each 6 mm diameter pupil for computing the corresponding point-spread function by conventional Fourier optics techniques.

Individual SH spot images were analyzed to determine their size and regional variation over the pupil. Because micro-aberrations and light scatter encountered on the first pass of the SH system will uniformly blur all SH spot images,[24] regional increases in the double-pass size of SH spots are a measure of micro-aberrations and scatter encountered on the second pass. Spot size was quantified by the equivalent width (EW), defined as the diameter of the circular base of a cylinder with the same height and volume as the distribution of light intensity within the spot.[35] The EW quantifies micro-aberrations that modulate wavefront slope across each lenslet,[24] but it does not fully capture wide-angle optical scatter such as that associated with cataracts.[36,37] All aberration and scatter analysis was performed using custom MATLAB programs.

Spatial Correlation Analysis between TBU and Optical Aberrations

Digital FL and RI images were obtained from video-capture of slit lamp images. Regions of TBU were identified in the FL images by thresholding based on pixel luminance, using custom MATLAB programs.[38] TBU areas in the RI images were identified as regions containing the characteristic intensity fluctuations associated with TBU using Image J (http://rsbweb.nih.gov).[29] TBU regions were identified in the raw SH images as those areas with missing, blurred, and/or highly displaced spots. Mapping of TBU regions from raw SH images was performed by observers unaware of subject identification or the appearance of FL or RI images. FL images were masked to the pupil for comparison to SH and RI images. Registration of TBU maps was complicated by small eye movements and pupil size fluctuations that occurred during the short intervals between these sequential measurements. Therefore, images were adjusted to find the position that achieved maximum TBU map overlap. Overlap of the TBU regions was calculated for pairs of SH and FL TBU maps and SH and RI TBU maps obtained at similar times within individual periods of blink suppression.

RESULTS

One of the primary goals of this study was to determine the extent to which TBU is manifest in the two finer scales of aberrations (macro-VHOA and micro-aberrations) not included in conventional modal analysis of HOA. In order to link regional optical changes to disruption of the tear film, a preliminary investigation was performed of the spatial correlation between TBU as manifest in three clinical imaging modalities: fluorescein (FL), retroillumination (RI) and SH wavefront aberrometry.

Spatial correlation of TBU with SH data images

TBU developed at the end of blink suppression trials in all eyes. Figure 2 shows an example from subject #1 of FL, RI, and SH images obtained at the beginning and end of a single trial. The FL image shows no TBU in the beginning and extensive TBU after refraining from blinking (Figures 2A and B). Dark areas in the FL image are traditionally interpreted as areas of TBU.[32] Intensity fluctuations in the RI image (Figures 2C and D) appear in the same general locations as TBU in the FL image (compare Figures 2B and 2D), which our group has previously shown to be spatially correlated.[29] Anomalies in the SH image after TBU (Figure 2F) also appear most obvious in the same general regions as TBU in the FL and RI images. Similar results after TBU for the other 4 subjects are shown in Figure 3. These images reveal the idiosyncratic nature of the FL patterns due to TBU in different eyes (Figures 3A-D).[2,38] However, despite the varied location of TBU and the fact that post-TBU measurements were recorded at different times after blinking, the general pattern and location of tear disruption in the FL images appears similar to RI (Figures 3E-H) and SH images (Figures 3I-L) for each subject.

In order to quantify the similarity of spatial location of TBU identified by FL and SH images, the percentage of overlap of TBU areas was calculated using the method demonstrated in Figure 4. Each image in Figure 4 was constructed by overlapping the thresholded FL image (areas of TBU indicated by stripes) with the SH image (areas indicated by dots) with any areas of overlap showing a combination of stripes and dots. The percent overlap (values in lower right corner of each image) was calculated by dividing the number overlap pixels by the number of pixels within the FL defined TBU regions. The area of FL TBU was used in the denominator because it is considered defines TBU in the traditional clinical sense.[32] For our study population of 5 subjects, the overlap ranged from 70-95%, with an average of 77% (SD=13%). Similar analysis was performed for the overlap TBU defined by intensity modulations in the RI images and disruptions in the SH images.

The range of overlap was 57-99%, with a mean of 74% (SD=17%). These results reveal that missing, displaced, and/or blurred spots in raw SH images occur predominantly within areas of TBU defined by reduced fluorescence. Since the FL, RI and SH images were not recorded at exactly the same time, the high spatial correlation indicates that regions of TBU remain stable over time if there are no blinks.

An example of the spatial overlap of TBU in FL images with the wavefront aberration map derived from the displacement of SH spots using the zonal reconstruction method is shown in Figure5 for subject #1. The wavefront map has been aligned to the pupil in the FL image. Theory predicts that the exiting wavefront will appear phase advanced due to a decrease in optical path length in regions of tear thinning or TBU. Conversely, phase retardation should occur in areas of relatively thick tears (or possibly an increase in refractive index) where the optical path length is relatively long. As predicted, phase advancement (positive wavefront error) occurred in areas of TBU relative to areas where tears are still intact (negative wavefront error).

Effect of TBU on Macro-aberrations

The effect of TBU on macro-aberrations of all three scales: lower order aberrations (LOA), higher-order aberrations (HOA), and very-high-order aberrations (VHOA), is illustrated in Figure 6 for Subject #1. The first two rows show the wavefront error maps reconstructed by the modal and zonal methods. Both reconstruction methods revealed new features in the WFE maps after TBU that indicate increased aberrations associated with TBU. As expected, the zonal map reveals a similar overall but somewhat more irregular pattern than the smoothed modal map. The magnitude of increased wavefront aberration associated with TBU, as quantified by the RMS of the modal wavefront, is consistent with the literature.[1,4,6-9,39] The modal WFE map is the sum of two other maps (LOA, HOA) displayed in the third and fourth rows. The VHOA map displayed in the fifth row is the difference between the zonal and modal maps. In this eye RMS after TBU increased by a factor of 3.5(HOA) and 2.9 (VHOA) compared to modest increase in LOA (ratio of 1.4). Similarly, the absolute changes in RMS for HOA (0.47 microns) and for VHOA (0.37 microns) for this subject were both greater than the change in LOA (0.26 microns). This LOA ratio may in fact be an overestimate of the TBU effect because the spherical defocus change observed in the LOA might be due in part to accommodation rather than TBU. Table 1 summarizes the changes in macro-aberrations for all subjects before and after TBU. All five subjects showed an increase in optical aberrations at all spatial scales following TBU. The average relative increase in RMS after TBU for the five subjects in this study was larger for HOA (1.90, SD=0.87) and VHOA (2.94, SD=1.07) than for LOA (1.48). With the exception of subject #3, the absolute change in HOA and VHOA was also greater than for LOA. Taken together, these results indicate that the optical effect of sustained blink suppression on macro-aberrations is larger at the finer spatial scales.

The impact of different scales of macro-aberrations on retinal image quality can be evaluated by examining the computed point spread functions derived from measured wavefronts after select orders of aberrations have been computationally corrected. The wavefront determined by the zonal fitting method was subtracted from the wavefronts generated by a select number of Zernike modes. PSF are then computed using standard Fourier methods from these remaining WFE maps, which include all of the macro-aberrations that have not been corrected. Three examples of this approach are shown in Figure 7. Soon after blinking (“Baseline” data, left hand column), the PSF computed with all LOAs corrected is dominated by the three-lobed trefoil, and after correcting all modes $\leq 4^{th}$ order a small central core in the PSF emerges that is similar to the central core observed when all orders up to the 10^{th} are corrected (bottom left panel). In these latter two cases, the impact of the remaining uncorrected HOAs can be seen as PSF intensity beyond this central

core. For comparison, a diffraction limited PSF for the 6 mm pupil used in these analyses is shown as an inset in the bottom left panel. These PSF computations show that, in the presence of an intact tear film, macro-aberrations lower than 5th order can prevent a high intensity core forming in the PSF. In contrast to these baseline data, the PSFs computed from post-TBU wavefronts (center and right hand column in Figure7 show examples from 2 different eyes) fail to develop a single high intensity core even when macro-aberrations up to the 10th order have been corrected (Figure 7) showing the importance of the VHOA (those beyond 10th order) in degrading retinal image quality after TBU.

Effect of TBU on micro-aberrations

Close inspection of the raw SH images in Figures 2 and 3 shows blurring and enlargement as well as displacement of some SH spot images after TBU. For example, Figure 8 shows an enlarged portion of the SH spot images from the subject in Figure 2. Before TBU, spot images are well focused and form a highly regular pattern (Figure 8A), but after TBU many spot images are noticeably blurred (Figure 8D) and peak intensity is greatly reduced. To determine the extent to which this blurring of individual spots can be accounted for by macro-aberrations, the expected image was computed as predicted by diffraction effects plus the wavefront errors over the face of the corresponding lenslet.[24,39] The modal wavefront map for this purpose was used with Zernike interpolation of wavefront values over the lenslet face. These computed spot images are shown in Figures 8C and F for the same lenslets responsible for the spot images displayed in Figures 8B and E. Prior to TBU, the computed spot image (Figure 8C) is very similar to that expected from double pass through a diffraction limited system with a 1 mm entry beam and a 0.4 mm square lenslet aperture on the second pass.[24] The close agreement between the observed and calculated baseline images provides evidence that SH spot quality in an eye with a high quality tear film is limited primarily by diffraction and macro-aberrations. In contrast, many of the spot images after TBU are significantly more blurred (e.g. in Figure 8 compare E with F) than expected based upon the HOAs and diffraction. This result implies that the blur seen in SH spot images after TBU is due primarily to the combined effect of increased VHOA plus micro-aberrations beyond the resolution of the aberrometer (Figure 1). Since blurring of SH spots is due primarily to micro-aberrations, the levels of micro-aberrations were quantified using the equivalent width (EW)of each spot image.[35] If both optical paths in our double pass SH system were diffraction limited, then SH spots that are not located within areas of TBU should have an equivalent width (EW) of 9.7 arc minutes in our system (1 mm beam entering eye and a lenslet diameter of 0.4 mm in the exiting beam).[24]Experimentally the EW of the least blurred SH spot images before TBU was found to be approximately 10-12 arc minutes, which is close to the diffraction-limited prediction. The average EW increased to 16 arc minutes after TBU, but this average includes regions of TBU and regions with intact tears. The spatial distribution of these EW increases after TBU was examined by mapping the EW magnitudes across the pupil (Figure 9). Regions where blurring of spots was greatest matched the TBU regions for these eyes shown in Figures 2 and 3 and also matched the TBU/SH overlap maps shown in Figure 4. Frequency histograms of EW values in a SH image were unimodal before TBU, but after TBU the magnitudes of EW typically formed a bimodal distribution. That is, EWs were either very large within regions of TBU (range approximately 30 to 40 arcminutes) or else much smaller in regions with intact tears prior to TBU (10 to 20 arcminutes). These results indicate that TBU caused by sustained blink suppression can also increase the eye's micro-aberrations that exist on a spatial scale smaller than the 0.4mm diameter of the lenslets used in our SH aberrometer.

DISCUSSION

The primary goal of this study was to measure the spatial distribution and scale of optical aberrations produced by thinning and TBU. To do so, periods of blink suppression were purposefully extended to allow the full range of TBU and its optical consequences to be studied. The principal finding is that degradation of the tear film's optical quality after sustained blink suppression causes wavefront aberrations on all four spatial scales enumerated: LOA, HOA, VHOA, and micro-aberrations smaller than the 0.4mm width of the lenslets used in our aberrometer. Although blink suppression was artificially extended in this study, the results suggests that prior clinical studies that reported only LOA and HOA wavefront aberrations of the tear film[2,8,9,27,39] could have under-reported the full extent of optical effects of TBU because no other optical aberrations were considered. The missing components of a conventional modal analysis are the very-high-order macro-aberrations (VHOA) that are measured by wavefront sensors but not included in the Zernike model plus scatter generated by micro-aberrations.[24,26,36,39] Computed retinal PSFs after typical HOAs have been corrected (Figure 7) emphasize that VHOAs create significant image blur after TBU. Also, this study demonstrated major increases of spot size in the raw SH images in the same tear film locations where FL images are dark (Figures 2 & 3), showing that scatter-producing micro-aberrations emerge after the tear film dissipates. These light-scattering aberrations in regions of extensive TBU may be caused by exposure of the microscopically rough epithelial surface or an epithelial surface covered by mucins or other tear remnants (proteins, lipids, etc).[40]A similar situation has been observed in the SH spot images of eyes with cataracts, which reveal a spatial map of forward light scatter caused by the cataract.[36,39,41] SH spot image blur in these eyes has been attributed to narrow angle scatter caused by microscopic optical disturbances larger than the wavelength of light.[39] However, if the optical characteristics of TBU include wide angle scatter (as observed with cataracts[36,39]), much of the scattered light may not reach the image plane of the SH aberrometer,[24] and the resulting spot images will have less light (e.g. see examples of missing spots in Figure 3).

While the extensive TBU observed in our study is unlikely to occur under normal conditions for the healthy eye, there is evidence that the highly unstable and inadequate tear film of dry eye subjects may experience micro-aberrations.[42,43] Several studies have shown that extensive tear break-up occurs in dry eye and contact lens wearers, especially when engaged in tasks requiring concentration, when blinking can be incomplete or slowed by as much as a factor of 10.[44-46]Therefore, the blink suppression paradigm used in this study to demonstrate the full range of optical aberrations may serve as a model for the full scope of optical changes that are possible with tear instability. Moreover, studying the optical consequences of extensive tear break-up underscored the optical role played by an intact tear film in the normal, healthy eye.

Mydriatics and anesthetic were instilled into test eyes to allow extended blink suppression with the pupil large enough to obtain adequate wavefront data. It is possible that these pharmaceutical agents may have affected tear film stability and thus the time course, distribution and extent of TBU. In addition, subjects moved sequentially through FL, SH and RI imaging in this study, so eye movements or head position could have had some effect on our data, although it was minimized by training and alignment of images by the center of the pupil. This failure to capture the different images of the tear film simultaneously may have contributed to the less than perfect (<100%) spatial correspondence in the TBU regions identified by each method (Figure 4).

In summary, optical aberrations at all spatial scales measured by the SH aberrometer developed in the same spatial location as TBU during periods of blink suppression and

contributed to reduced optical quality of the eye. Our results suggest that the optical signature of tear break-up can include a combination of wavefront aberrations on macroscopic and microscopic scales due to non-uniform tear film thinning and exposure of a rough epithelial surface. Thus, these aberrations are likely to be a primary cause of the loss of retinal image quality that has been postulated previously to explain symptoms of visual disturbances reported by dry eye patients.

Acknowledgments

We gratefully acknowledge the support of Xin Hong and Kevin Haggerty for computer programming used in data analysis. This project was supported by NEI Grant R01-EY05109 (LNT), 1R01EY021794-01 (CGB), and Indiana CTSI Career Development Award KL2RR025760-01(NLH).

REFERENCES

1. Thibos LN, Hong X. Clinical applications of the Shack-Hartmann aberrometer. Optom Vis Sci. 1999; 76:817–25. [PubMed: 10612402]
2. Liu H, Begley CG, Chalmers R, Wilson G, Srinivas SP, Wilkinson JA. Temporal progression and spatial repeatability of tear breakup. Optom Vis Sci. 2006; 83:723–30. [PubMed: 17041317]
3. Ferrer-Blasco T, Garcia-Lazaro S, Montes-Mico R, Cervino A, Gonzalez-Meijome JM. Dynamic changes in the air-tear film interface modulation transfer function. Graefes Arch Clin Exp Ophthalmol. 2010; 248:127–32. [PubMed: 19779931]
4. Liu H, Thibos L, Begley CG, Bradley A. Measurement of the time course of optical quality and visual deterioration during tear break-up. Invest Ophthalmol Vis Sci. 2010; 51:3318–26. [PubMed: 20107168]
5. Montes-Mico R. Role of the tear film in the optical quality of the human eye. Journal of cataract and refractive surgery. 2007; 33:1631–5. [PubMed: 17720082]
6. Xu J, Bao J, Deng J, Lu F, He JC. Dynamic changes in ocular Zernike aberrations and tear menisci measured with a wavefront sensor and an anterior segment OCT. Invest Ophthalmol Vis Sci. 2011; 52:6050–6. [PubMed: 21613369]
7. Li KY, Yoon G. Changes in aberrations and retinal image quality due to tear film dynamics. Opt Express. 2006; 14:12552–9. [PubMed: 19529690]
8. Koh S, Maeda N, Hirohara Y, et al. Serial measurements of higher-order aberrations after blinking in normal subjects. Invest Ophthalmol Vis Sci. 2006; 47:3318–24. [PubMed: 16877397]
9. Montes-Mico R, Alio JL, Charman WN. Dynamic changes in the tear film in dry eyes. Invest Ophthalmol Vis Sci. 2005; 46:1615–9. [PubMed: 15851559]
10. Tutt R, Bradley A, Begley C, Thibos LN. Optical and visual impact of tear break-up in human eyes. Invest Ophthalmol Vis Sci. 2000; 41:4117–23. [PubMed: 11095604]
11. Goto E, Yagi Y, Matsumoto Y, Tsubota K. Impaired functional visual acuity of dry eye patients. Am J Ophthalmol. 2002; 133:181–6. [PubMed: 11812420]
12. Ridder WH 3rd, LaMotte J, Hall JQ Jr. Sinn R, Nguyen AL, Abufarie L. Contrast sensitivity and tear layer aberrometry in dry eye patients. Optom Vis Sci. 2009; 86:E1059–68. [PubMed: 19648840]
13. Thai LC, Tomlinson A, Ridder WH. Contact lens drying and visual performance: the vision cycle with contact lenses. Optom Vis Sci. 2002; 79:381–8. [PubMed: 12086305]
14. Toda I, Yoshida A, Sakai C, Hori-Komai Y, Tsubota K. Visual performance after reduced blinking in eyes with soft contact lenses or after LASIK. J Refract Surg. 2009; 25:69–73. [PubMed: 19244954]
15. Begley CG, Caffery B, Nichols KK, Chalmers R. Responses of contact lens wearers to a dry eye survey. Optom Vis Sci. 2000; 77:40–6. [PubMed: 10654857]
16. Begley CG, Chalmers RL, Mitchell GL, et al. Characterization of ocular surface symptoms from optometric practices in North America. Cornea. 2001; 20:610–8. [PubMed: 11473162]

17. Aakre BM, Doughty MJ. Are there differences between ‘visual symptoms’ and specific ocular symptoms associated with video display terminal (VDT) use? Cont Lens Anterior Eye. 2007; 30:174–82. [PubMed: 17293157]
18. Martin R, Sanchez I, de la Rosa C, et al. Differences in the daily symptoms associated with the silicone hydrogel contact lens wear. Eye Contact Lens. 2010; 36:49–53. [PubMed: 20009943]
19. The definition and classification of dry eye disease: Report of the Definition and Classification Subcommittee of the International Dry Eye WorkShop. The ocular surface. 2007; 5:75–92. 2007. [PubMed: 17508116]
20. Mertzanis P, Abetz L, Rajagopalan K, et al. The relative burden of dry eye in patients’ lives: comparisons to a U.S. normative sample. Invest Ophthalmol Vis Sci. 2005; 46:46–50. [PubMed: 15623753]
21. Schiffman RM, Christianson MD, Jacobsen G, Hirsch JD, Reis BL. Reliability and validity of the Ocular Surface Disease Index. Arch Ophthalmol. 2000; 118:615–21. [PubMed: 10815152]
22. Miljanovic B, Dana R, Sullivan DA, Schaumberg DA. Impact of dry eye syndrome on vision-related quality of life. Am J Ophthalmol. 2007; 143:409–15. [PubMed: 17317388]
23. Panagopoulou SI, Neal DR. Zonal matrix iterative method for wavefront reconstruction from gradient measurements. J Refract Surg. 2005; 21:S563–9. [PubMed: 16209462]
24. Nam J, Thibos LN, Bradley A, Himebaugh N, Liu H. Forward light scatter analysis of the eye in a spatially-resolved double-pass optical system. Opt Express. 2011; 19:7417–38. [PubMed: 21503052]
25. Goodman, JW. Statistical Optics. Wiley; New York, NY: 2000.
26. Benito A, Perez GM, Mirabet S, et al. Objective optical assessment of tear-film quality dynamics in normal and mildly symptomatic dry eyes. Journal of cataract and refractive surgery. 2011; 37:1481–7. [PubMed: 21782090]
27. Montes-Mico R, Alio JL, Munoz G, Charman WN. Temporal changes in optical quality of air-tear film interface at anterior cornea after blink. Invest Ophthalmol Vis Sci. 2004; 45:1752–7. [PubMed: 15161836]
28. Thibos LN. Principles of Hartmann-Shack aberrometry. J Refract Surg. 2000; 16:S563–5. [PubMed: 11019873]
29. Himebaugh NL, Wright AR, Bradley A, Begley CG, Thibos LN. Use of retroillumination to visualize optical aberrations caused by tear film break-up. Optom Vis Sci. 2003; 80:69–78. [PubMed: 12553546]
30. Rubinstein J, Wolansky G. Reconstruction of optical surfaces from ray data. Optical Review. 2001; 8:281–3.
31. Cannon R. Global wave-front reconstruction using Shack-Hartmann sensors. JOSA A. 1995; 12:2031–9.
32. Norn MS. Desiccation of the precorneal film. I. Corneal wetting-time. Acta Ophthalmol. 1969; 47:865–80. [PubMed: 4187469]
33. Salmon TO, Thibos LN, Bradley A. Comparison of the eye’s wave-front aberration measured psychophysically and with the Shack-Hartmann wave-front sensor. J Opt Soc Am A Opt Image Sci Vis. 1998; 15:2457–65. [PubMed: 9729857]
34. Liang J, Grimm B, Goelz S, Bille JF. Objective measurement of wave aberrations of the human eye with the use of a Hartmann-Shack wave-front sensor. J Opt Soc Am A Opt Image Sci Vis. 1994; 11:1949–57. [PubMed: 8071736]
35. Thibos LN, Hong X, Bradley A, Applegate RA. Accuracy and precision of objective refraction from wavefront aberrations. Journal of vision. 2004; 4:329–51. [PubMed: 15134480]
36. Donnelly WJ 3rd, Pesudovs K, Marsack JD, Sarver EJ, Applegate RA. Quantifying scatter in Shack-Hartmann images to evaluate nuclear cataract. J Refract Surg. 2004; 20:S515–22. [PubMed: 15523968]
37. van den Berg TJ, Franssen L, Coppens JE. Straylight in the human eye: testing objectivity and optical character of the psychophysical measurement. Ophthalmic Physiol Opt. 2009; 29:345–50. [PubMed: 19422567]
38. Begley CG, Himebaugh N, Renner D, et al. Tear breakup dynamics: a technique for quantifying tear film instability. Optom Vis Sci. 2006; 83:15–21. [PubMed: 16432468]

39. Mihashi T, Hirohara Y, Bessho K, Maeda N, Oshika T, Fujikado T. Intensity analysis of Hartmann-Shack images in cataractous, keratoconic, and normal eyes to investigate light scattering. Jpn J Ophthalmol. 2006; 50:323–33. [PubMed: 16897216]

40. Gipson IK. Distribution of mucins at the ocular surface. Exp Eye Res. 2004; 78:379–88. [PubMed: 15106916]

41. Fujikado T, Kuroda T, Maeda N, et al. Light scattering and optical aberrations as objective parameters to predict visual deterioration in eyes with cataracts. Journal of cataract and refractive surgery. 2004; 30:1198–208. [PubMed: 15177593]

42. Goto T, Zheng X, Klyce SD, et al. Evaluation of the tear film stability after laser in situ keratomileusis using the tear film stability analysis system. Am J Ophthalmol. 2004; 137:116–20. [PubMed: 14700653]

43. Huang FC, Tseng SH, Shih MH, Chen FK. Effect of artificial tears on corneal surface regularity, contrast sensitivity, and glare disability in dry eyes. Ophthalmology. 2002; 109:1934–40. [PubMed: 12359618]

44. Jansen ME, Begley CG, Himebaugh NH, Port NL. Effect of contact lens wear and a near task on tear film break-up. Optom Vis Sci. 2010; 87:350–7. [PubMed: 20351601]

45. Himebaugh NL, Begley CG, Bradley A, Wilkinson JA. Blinking and tear break-up during four visual tasks. Optom Vis Sci. 2009; 86:E106–14. [PubMed: 19156014]

46. Doughty MJ. Consideration of three types of spontaneous eyeblink activity in normal humans: during reading and video display terminal use, in primary gaze, and while in conversation. Optom Vis Sci. 2001; 78:712–25. [PubMed: 11700965]

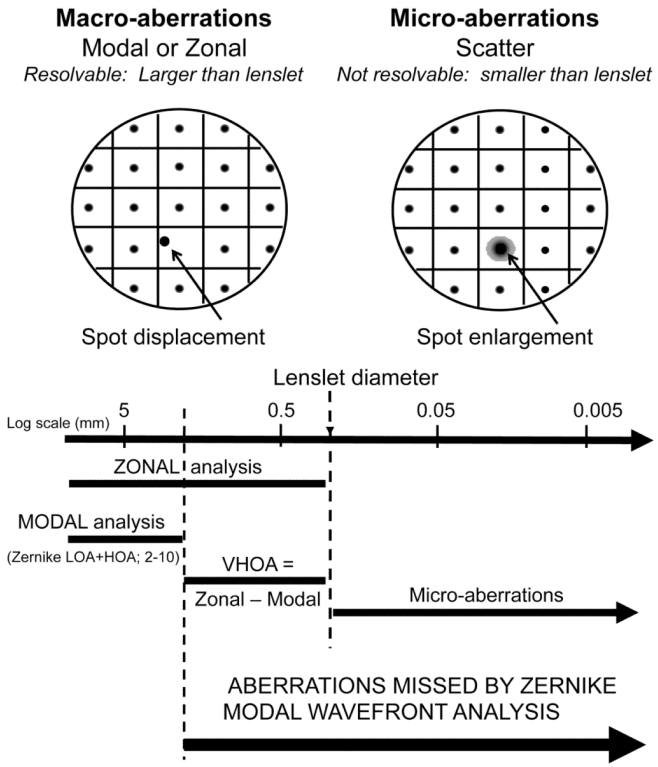

Figure 1.

Schematic raw SH data are shown in the top part of this figure. The left panel shows spot displacement (left arrow) as the basis of determination of macro-aberrations, while the right hand panel shows spot enlargement (right arrow) caused by micro-aberrations. The bottom half of this figure shows a size scale with courser aberrations on the left and finer aberrations on the right, quantified in mm in the pupil plane. The lines show the size range of macro-aberrations determined with either modal or zonal analysis, or from the difference between zonal and modal fitted wavefronts. Aberrations on a scale smaller than the lenslet diameter are indicated as micro-aberrations. The range of spatial scale missed by classic Zernike analysis is indicated by the thick black arrow.

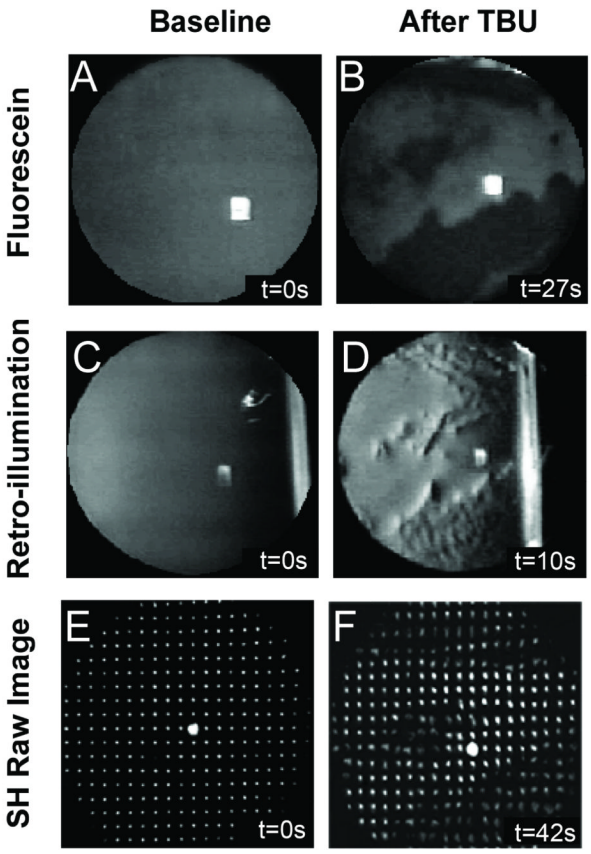

Figure 2.
Sample data images obtained with fluorescein (A and B), retroillumination (C and D) and SH aberrometry (E and F). Images are examples from Subject #1 at baseline (left) and after significant TBU (right). The time after the last blink (in seconds) is indicated in the bottom right hand corner of each panel.

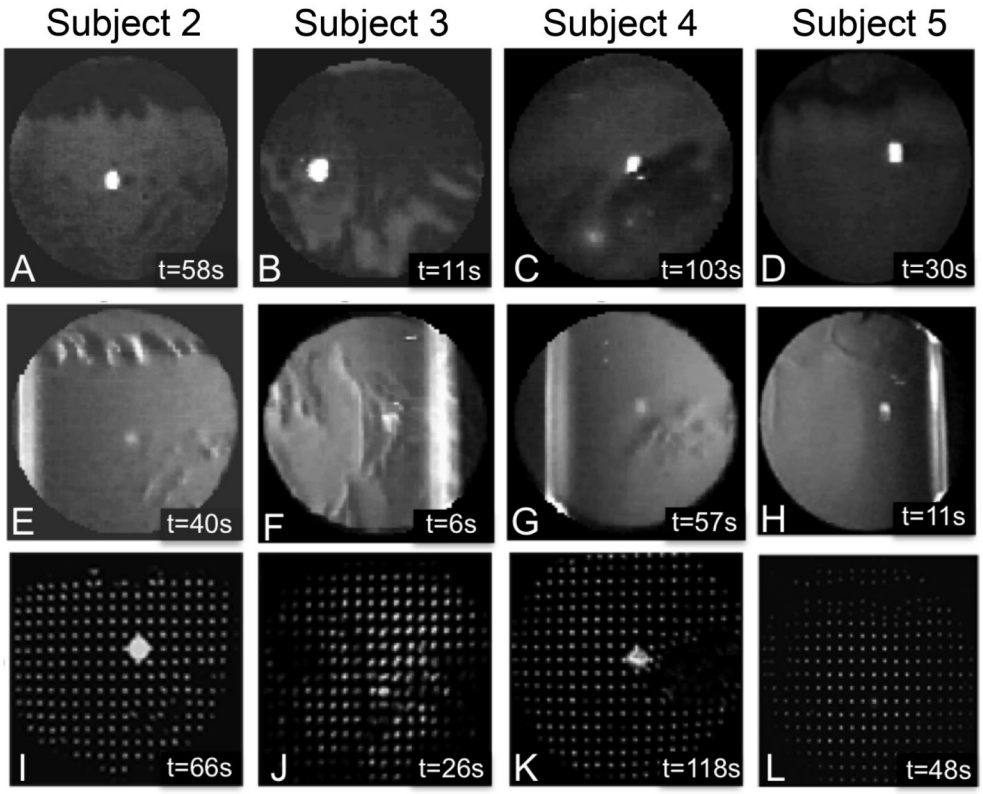

Figure 3.
Fluorescein (top row), retroillumination (middle row) and SH images (bottom row) after significant TBU for subjects 2-5. The time of data acquisition (in seconds) after the last blink is indicated in the bottom right hand corner of each panel.

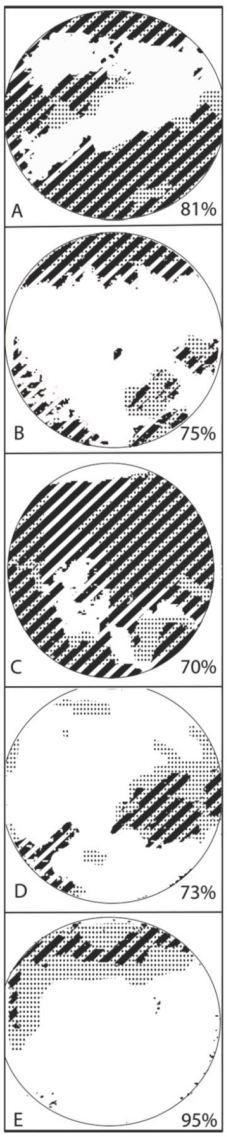

Figure 4.
Pupil maps showing regions of TBU determined with fluorescein imaging (stripes), SH aberrometry (dots) and regions that are common to both images (stripes + dots). The percent overlap was calculated with respect to fluorescein TBU (Overlap area/Fluorescein area) and is indicated in the bottom right hand corner of each panel. From the top, the subject numbers are 1,2,3,4,5.

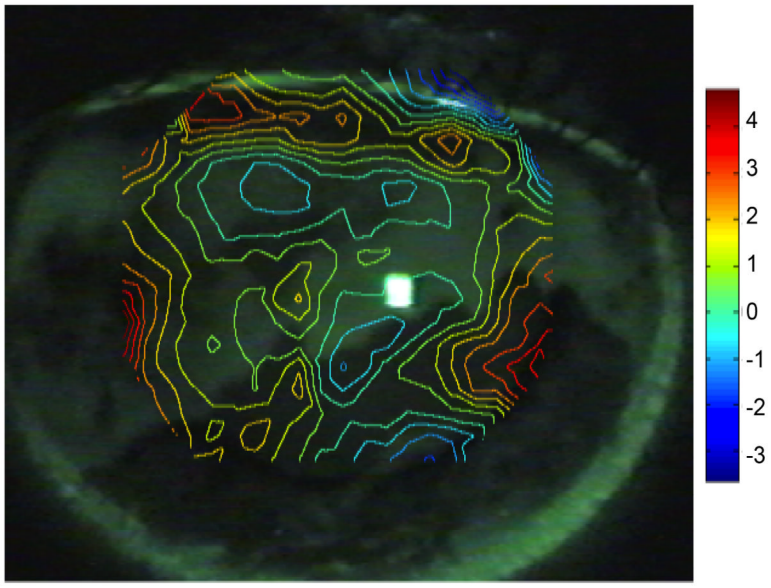

Figure 5.
Contour map showing WFE phase advance (hot colors) and retardation (cool colors) across the pupil of subject #1 after TBU overlaid over the post-TBU fluorescein image from the same eye. WFE map was determined using the zonal reconstruction method, and the scale bar indicates phase errors in microns relative to the pupil center.

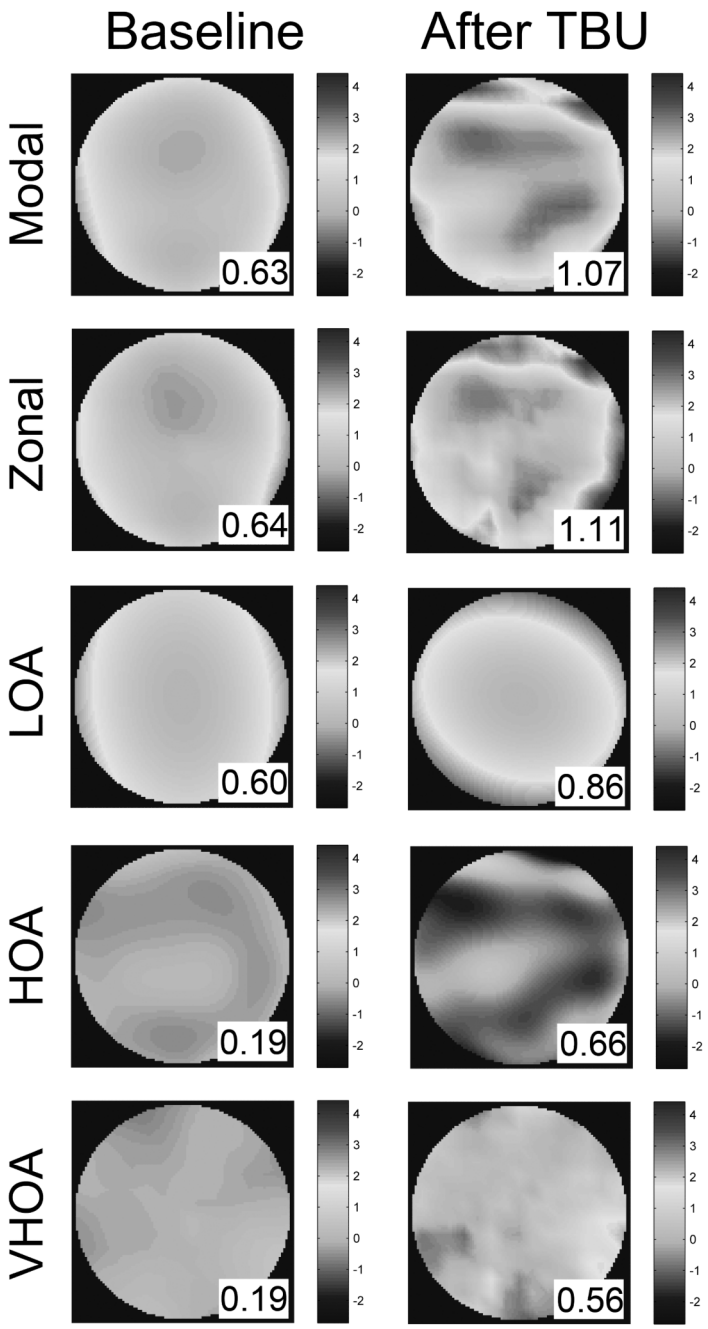

Figure 6.

WFE maps across the pupil of subject #1 at baseline (left) and after significant TBU (right) determined with different computational approaches. The root mean square (RMS) value of each wavefront is indicated in the bottom right of each map. Rms values (insert in each panel) were obtained by either modal (row1) or zonal (row2) methods which were then used to identify the rms contributed by three different scales of aberration: LOA (Zernike order 2), HOA (Zernike order 3-10), and VHOA (zonal – modal wavefront). See Rationale section for definitions of each fitting method and aberration scale.

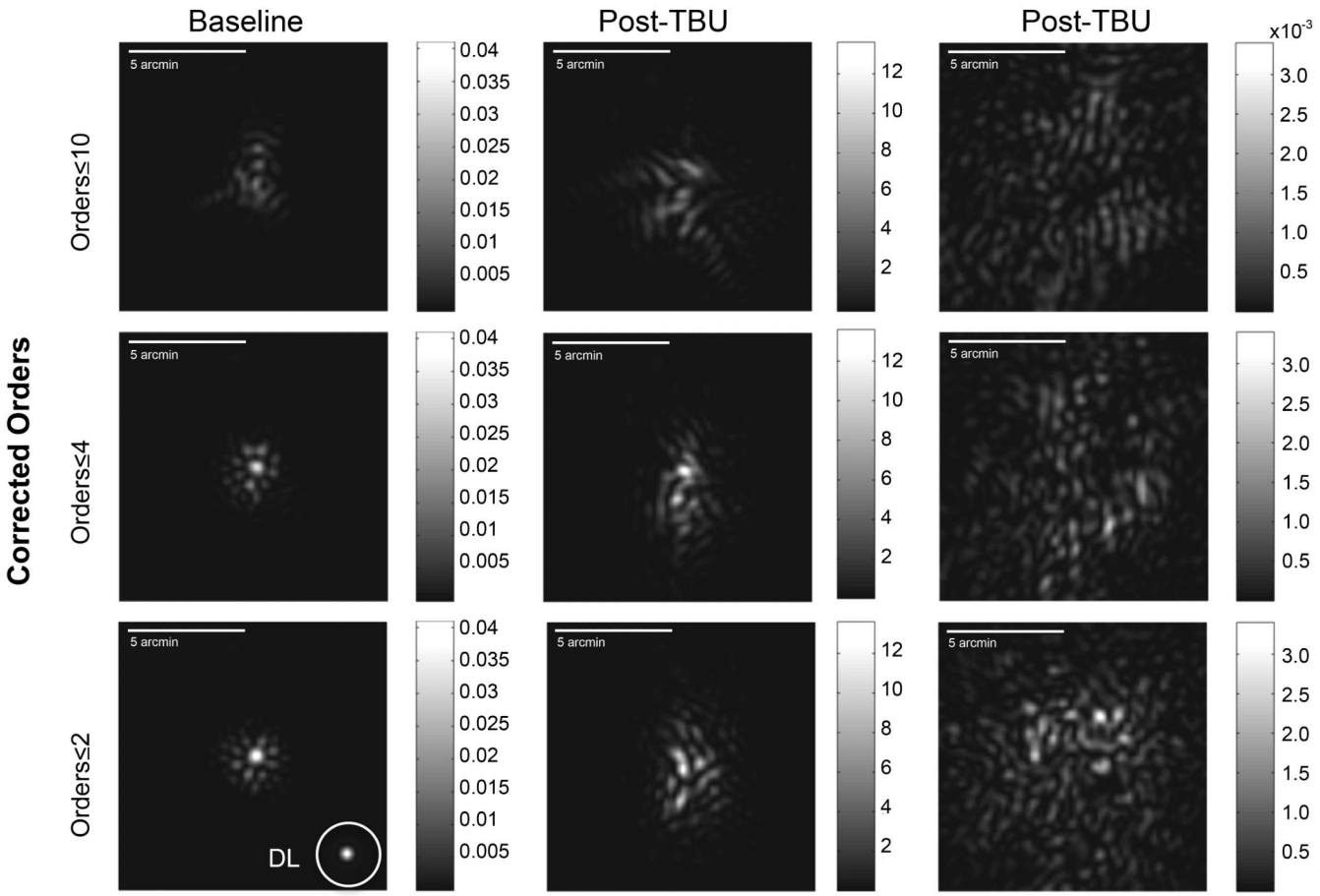

Figure 7.

Computationally simulated retinal PSFs were calculated from the zonal WFE maps obtained at baseline and after prolonged tear break-up (TBU) after either Zernike orders ≤2 , ≤4, or ≤10 were corrected by subtracting the WFEs determined by Zernike modes ≤2 , ≤4, or ≤10 from the zonal WFE maps. Sample data from a WFE map obtained soon after a blink (baseline) are shown in the left hand column, and examples of retinal PSFs computed from post-TBU wavefronts are shown in the center (less severe TBU) and right (more severe TBU) columns.

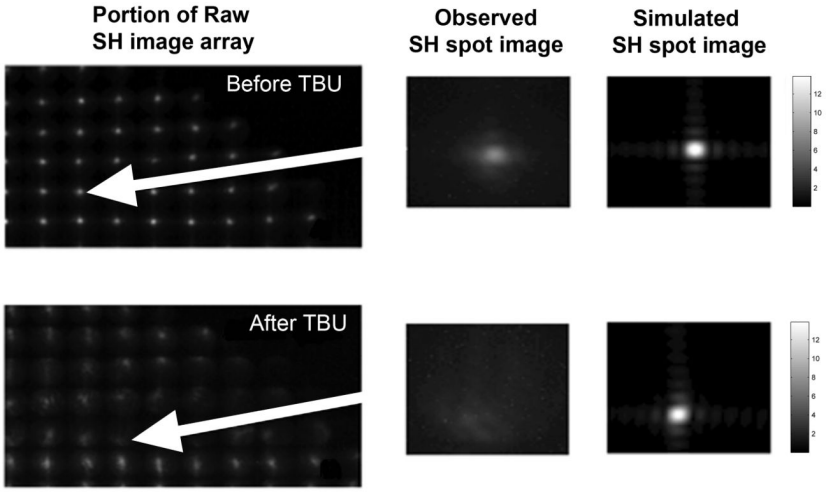

Figure 8.

Magnified views of individual and collections of raw SH point images obtained from subject #1 at baseline (top panels) or after TBU (bottom panels). Panels B and E show individual spot images extracted from the raw SH images (A and D) as indicated by the red arrows. Panels C and F show the same individual spot image computed using a computational SH simulator over a lenslet square aperture that employed the same wavelength and pupil size used in the experiment and included the same diffraction effects and the contribution to spot blur from the modal fitted HOAs. The square root transformation has been applied to spot images for display purpose. Equivalent widths for original double pass spot images (B and E) are 16 arcmin and 24 arcmin for the baseline and the tear break-up, respectively. Equivalent widths for simulated second pass spot images (C and F) are 6 arcmin and 6.8 arcmin for the baseline and the tear break-up, respectively.

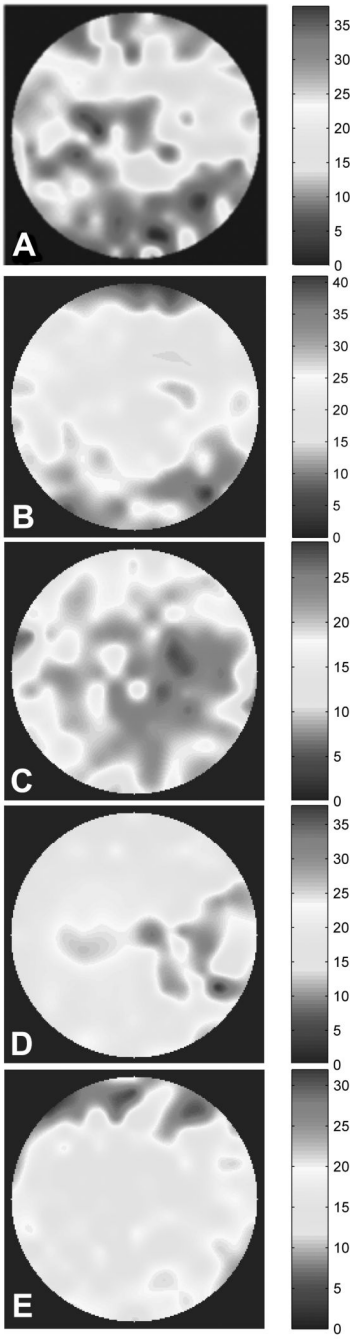

Figure 9.
Pupil maps for all 5 eyes quantifying SH spot image blur as EW in minutes of arc. Hot and dark colors indicate more spot image blur. Color scale for each image is slightly different and included for each panel. From the top, subject numbers are 1,2,3,4,5.

Table 1

Summary of wavefront RMS (microns) at baseline and after extensive tear break-up for five eyes. RMS of wavefronts reconstructed by either modal (column 1) or zonal (column 2) methods are used to compute the RMS contributed by three different scales of aberration: LOA (Zernike order 2), HOA (Zernike orders 3-10), and VHOA (zonal – modal wavefront). See the Rationale section of Methods for descriptions of analysis methods and aberration scales. Also included (in parentheses) are the ratios and differences of RMS after TBU compared to the baseline data. Averages for all 5 eyes are in the bottom row.

Tear breakup/baseline (ratio, difference)					
Subject	**MOD**	**ZON**	**LOA**	**HOA**	**VHOA**
1	1.07/0.63 (1.7, 0.44)	1.11/0.64 (1.7, 0.47)	0.86/0.60 (1.4, 0.26)	0.66/0.19 (3.5, 0.47)	0.56/0.19 (2.9, 0.37)
2	0.86/0.77 (1.1, 0.09)	0.88/0.76 (1.2, 0.12)	0.72/0.68 (1.1, 0.04)	0.50/0.33 (1.5, 0.17)	0.28/0.15 (1.9, 0.13)
3	3.23/1.28 (2.5, 1.95)	3.26/1.29 (2.5, 1.97)	3.12/1.25 (2.5, 1.87)	0.56/0.39 (1.4, 0.17)	0.69/0.15 (4.6, 0.54)
4	1.31/1.08 (1.2, 0.23)	1.29/1.09 (1.2, 0.20)	1.19/0.99 (1.2, 0.20)	0.70/0.46 (1.5, 0.24)	0.56/0.18 (3.1, 0.38)
5	0.86/0.70 (1.2, 0.16)	1.04/0.75 (1.4, 0.29)	0.78/0.66 (1.2, 0.12)	0.44/0.27 (1.6, 0.17)	0.46/0.21 (2.2, 0.25)
Average	1.54, 0.56	1.6, 0.61	1.48, 0.50	1.90, 0.24	2.94, 0.33